Valence capture mechanism in resonance neutron capture by ^{13}C

S. Raman
Japan Atomic Energy Research Institute, Tokai-mura, Naka-gun, Ibaraki-ken, Japan
and Oak Ridge National Laboratory, Oak Ridge, Tennessee 37831

M. Igashira, Y. Dozono, and H. Kitazawa
Research Laboratory for Nuclear Reactors, Tokyo Institute of Technology, O-okayama, Meguro-ku, Tokyo, Japan

M. Mizumoto
Japan Atomic Energy Research Institute, Tokai-mura, Naka-gun, Ibaraki-ken, Japan

J. E. Lynn*
Argonne National Laboratory, Argonne, Illinois 60439
(Received 7 August 1989)

The partial radiation widths of three (two electric dipole and one electric quadrupole) primary γ transitions in ^{14}C, subsequent to neutron capture by the 153-keV, 2^+ resonance in ^{13}C, have been remeasured. Both electric dipole transitions, accounting for more than 80% of the total radiation width, can be explained as valence neutron transitions. The deduced total radiation width of $0.215^{+0.084}_{-0.035}$ eV for this resonance disagrees with the previous value of 2.4 ± 0.9 eV and significantly affects the production of $A \geq 14$ nuclei in primordial nucleosynthesis.

I. INTRODUCTION

In a number of recent papers,[1-7] the evidence for and the relative importance of the operation of a direct mechanism in slow-neutron capture have been carefully studied for a range of light nuclides. It has been concluded that for ^{9}Be, ^{12}C, ^{13}C, the sulfur isotopes ($^{32,33,34,36}S$), and the even calcium isotopes ($^{40,42,44,48}Ca$), at thermal-neutron energies, direct capture is the predominant mechanism for generating the significant electric-dipole ($E1$) transitions. The calculated cross sections from the direct-capture theory, quantitatively formulated within an optical-model framework, are mostly in fair agreement with the measured values. The remaining discrepancies could be assigned plausibly to a much smaller (on average) contribution from a compound-nucleus mechanism operating through the tails of local levels affecting the initial state and staying uncorrelated with the single-particle content of the initial or final state.

In its most developed form (Ref. 1, 3, and 4), the theory of direct capture expresses the capture amplitude as the sum of two terms—a potential-capture amplitude and a valence-capture amplitude. The former is due to the single-particle motion of the projectile neutron in the potential field of a global optical model and the latter is due to the projection of the single-particle motion in the wave function of local resonance levels. The magnitude of the contribution from the local levels can be assessed from the difference between the calculated (from the optical model) potential scattering length and the measured scattering length of the target nucleus. In the cases that we have studied until now, the valence term is often an important (though not the larger) contribution. Thus, the valence amplitude is apparently an important component of resonance neutron capture for most of the light nuclides listed above; it also appears to account[1] for most of the total radiation width of the 102.7-keV resonance of ^{32}S.

Through direct measurements of radiative transitions from resonances, valence capture has also been established as being a significant process for a few medium-mass nuclides ($50 \leq A \leq 100$), namely $^{92,98}Mo$ (Ref. 8), ^{54}Fe (Refs. 9 and 10), and ^{60}Ni (Ref. 10). However, in the case of resonances in some isotopes, ^{100}Mo in particular,[11] the appearance of valence capture does not seem to be systematic. Because the studied resonances in ^{100}Mo are of p-wave character, this result may possibly indicate an orbital angular-momentum (l) effect on the strength of valence capture, and indeed it has been demonstrated that an important reason for the strength of potential and valence capture in the low-energy s-wave region is boundary-condition mixing that causes decoupling of low-l orbitals from the giant-dipole resonance.[12] Another suggested cause[13] is the nearly complete spreading of a low-l single-particle wave function into the channel and its subsequent isolation from the strong particle-hole mixing effects in the internal nuclear region. This mechanism draws electric-dipole strength away from the moderate energy regions excited by slow neutrons to the much higher excitation-energy region of the giant-dipole resonance.

To fully understand the mechanisms of neutron capture, it is, therefore, important to make many more absolute measurements of the partial radiation widths of neutron resonances over a wide range of nuclides, and preferably over as broad a range of neutron energy and orbital angular momentum as possible, in conjunction with a full analysis from the valence-model viewpoint. In this paper

we study an important resonance in the cross section of a very light nuclide,^{13}C. The resonance investigated is at 153 keV, it is of p-wave character, and has a large reduced neutron width. The experimental work on this resonance and other nuclear data required for the valence-model analysis are discussed in Sec. II.

The theoretical methods that have generally been used to calculate valence-capture widths stem from the optical-model formulation of direct capture. In the original formulation[14] for very low-energy neutron capture, it was pointed out that the real part of the radial matrix element calculated from the optical-model initial wave function would yield the potential-capture cross section; this is the cross section that would result when the contribution of local levels to the initial wave function was absent or negligible. The imaginary part of the radial matrix element could be interpreted as the average residue of a many-level interference term in the valence-capture term, and from this part an average valence radiation width could be deduced. This concept was later generalized[15] and it was shown that the same interpretation of real and imaginary parts would hold after extraction of an optical-model scattering phase-shift factor. This prescription for calculating the valence radiation width has been adhered to in most later work, especially since it has been believed that to follow a more direct calculational route is fraught with normalization difficulties. In fact, normalization is not a problem, despite the point made in Refs. 15 and 16 that the use of the single-particle matrix elements presented in Ref. 17 will give rise to incorrect normalization when used for calculating the contribution of the entrance channel to valence capture; the matrix elements of Ref. 17 were intended to give typical values for moderately bound (closed) channels in a much more general model of valence capture for estimating total radiation widths.

In this paper we base our calculation of the valence radiation width for the elastic-scattering channel on the $\mathcal{R}$-matrix theory of nuclear reactions. In this approach we require the assumption of a real potential to describe the single-particle states underlying the scattering, but avoid the necessity of formulating an imaginary term to describe the spreading of the single-particle state into the compound-nucleus states. The original formulation of radiation within this theory can be found in Ref. 18 and is also discussed in Ref. 17. The theory and the calculation of the radiation width of the resonance are described in Sec. III, where the results of theory and experiment are also compared. Implications of the current results for nucleosynthesis are discussed in Sec. IV, and a summary of this paper is provided in Sec. V.

II. MEASUREMENT OF THE RADIATION WIDTHS

A. Background

In the compilation of resonances,[19] the very first listing of a p-wave resonance below 1 MeV with a measured radiation width occurs in ^{13}C. This resonance is at 152.9 keV, it has a spin and parity assignment of 2^+ and a neutron width of $\Gamma_n = 3.7 \pm 0.7$ keV both from the work of Heaton *et al.*,[20] and its radiation width is quoted in Ref. 19 as $\Gamma_\gamma = 4.0 \pm 1.6$ eV. This radiation width comes from some of the earliest work carried out at the Oak Ridge Electron Linear Accelerator (ORELA) by Allen and Macklin.[21] The value quoted in Ref. 19 requires revision for three reasons: (1) the spin of this resonance has now been shown to be 2 instead of 1 as assumed in Ref. 21, (2) the equation relating the radiation width to the capture area was given incorrectly in Ref. 21, and (3) there exists now a better evaluation of the scattered neutron sensitivity for the detector system employed in Ref. 21. The last correction is especially serious[22] whenever the neutron width is large as is the case for the resonance under study. By reworking the old data, Macklin[23] has now obtained $\Gamma_\gamma = 2.4 \pm 0.9$ eV for the 152.9-keV, p-wave, $J = 2$ resonance in ^{13}C, the biggest change arising from reason (1) above.

There are, however, two reasons to seriously question the measured value of the radiation width for the 153-keV resonance. The first reason was raised by Ho and Castel[24] as follows. The expected decay scheme[25] of the 153-keV, 2^+ resonance is shown in Fig. 1. [Also shown there are the (d,p) spectroscopic factors from Refs. 26 and 27 needed for later use.] On empirical grounds,[28,29] the $M1$ transition at 1.31 MeV (see Fig. 1) and the $E2$ transitions at 1.73 and 8.32 MeV are all expected to be weak compared to the three $E1$ transitions of energies 2.22, 1.59, and 0.98 MeV. Of these three, the 2.22-MeV transition should be the strongest due to the E_γ^3 phase-space factor. Therefore, the 2.22-MeV transition most probably accounts for $\sim\frac{2}{3}$ of the total radiation width. The putative width of the 2.22-MeV transition is, therefore, ~ 1.6 eV or ~ 0.37 Weisskopf units. If correct, such a transition would represent one of the fastest $E1$ transitions ever observed.[30] This large value of ~ 1.6 eV radiation width can be also questioned for a second and more serious reason. Our preliminary calculations indicated that this width must be in error by about an order of magnitude. These calculations also suggested that any contemplated measurement of the partial radiation widths from the ^{13}C(n,γ) reaction would be very difficult indeed, and would require a γ-ray energy resolution sufficient to explicitly identify the γ rays in ^{14}C and thereby overcome some of the problems caused by the scattered neutrons being captured in extraneous materials. The resolution of the C_6F_6 detector employed in Ref. 21 was insufficient for this purpose and only the total radiation width was measured in that experiment.

B. Experimental procedure

The capture γ-ray measurements were made using a NaI(Tl) detector and time-of-flight (TOF) technique. The experimental arrangement is shown schematically in Fig. 2. Neutrons were generated by the ^{7}Li$(p,n)^7$Be reaction with a pulsed proton beam from the 3.2-MV Pelletron accelerator at the Tokyo Institute of Technology. The average proton-beam current was $10 \sim 13$ μA for a pulse repetition rate of 2 MHz and a pulse width of 1.5 ns. Neutrons incident on the sample were monitored by a ^{6}Li-glass scintillation detector located 40 cm from the

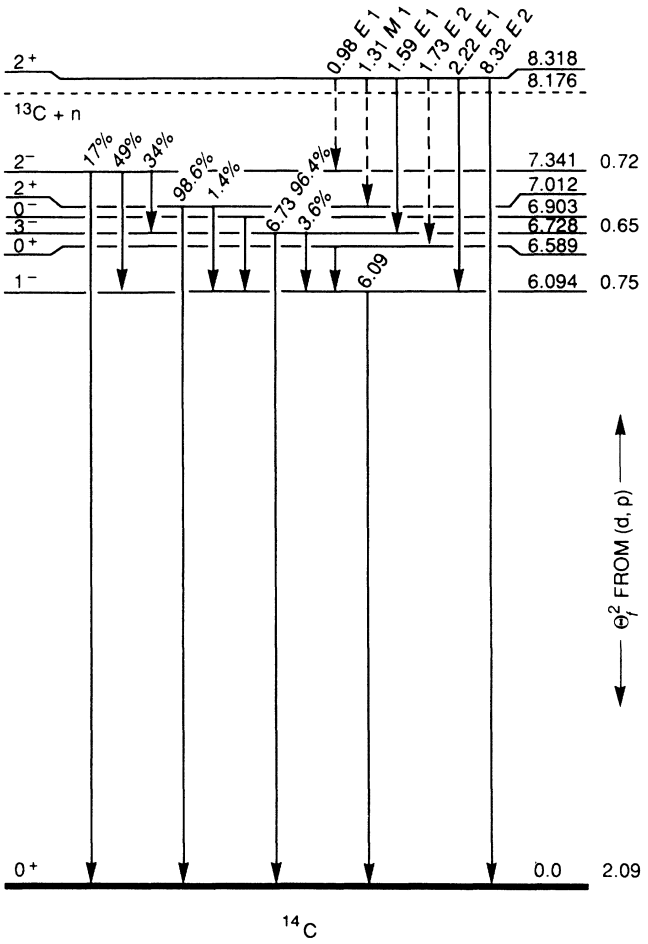

FIG. 1. Decay scheme of ^{14}C based mainly on Ref. 25. Of the six expected primary transitions from the capturing state at 8.318 MeV, only three (those at 8.32, 2.22, and 1.59 MeV) had intensities sufficient to be detected in this experiment. The corresponding secondary transitions at 6.09 and 6.73 MeV were also detected. The (d,p) spectroscopic factor (θ_f^2) for the ground state was from Ref. 26; those for all other levels from Ref. 27.

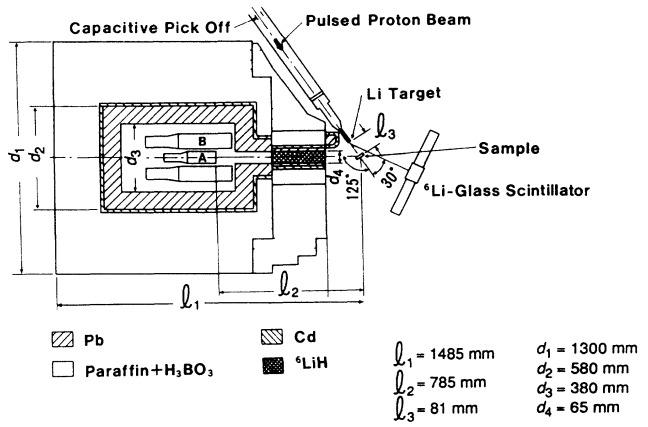

FIG. 2. Experimental arrangement employed to measure keV-neutron capture γ-ray spectra. The response of the anti-Compton NaI(Tl) detector is discussed in Ref. 31; the heavy shield in Ref. 32.

neutron source at an angle of 30° with respect to the direction of the proton beam. (All angles quoted in this section use this reference direction.) The ^{13}C sample was 99% enriched carbon powder in an acrylic resin container with dimensions of 5.8 cm diameter and 1.1 cm length. The isotopic thickness of ^{13}C was 0.0402 atoms/b in the direction of the neutron beam. This sample was located 8.1 cm from the neutron source at an angle of 0°. Capture γ rays from the sample were detected by a 7.6 cm diam and 15.2 cm long NaI(Tl) detector (A) centered in an annular NaI(Tl) detector (B) that was 25.4 cm in diameter and 28.0 cm in length. The entire detector assembly,[31] operated as an anti-Compton γray spectrometer, was placed in a heavy shield[32] consisting of borated paraffin, lead, and cadmium. A ^6LiH shield that absorbed effectively the neutrons scattered by the sample was added in the collimator of the detector shield. The distance between the sample and the spectrometer was 80 cm. Capture γ rays were observed at a laboratory angle of 125°. Because the second Legendre polynomial is zero at this angle, the differential measurement at this angle gave approximately the integrated γ-ray spectrum for the dipole transitions.

To obtain the relative total neutron spectrum incident on the sample, the TOF spectrum at the average angle of 14° was measured with the same ^6Li-glass detector employed earlier. The result is shown in Fig. 3 and the deduced neutron spectrum in Fig. 4. (The relative efficiency of the neutron detector was determined from a Monte Carlo calculation.[33,34]) Also shown in Fig. 4 are the neutron spectra at 0° (the center of the sample), 20° (the edge of the sample), and 30° (the angle where the neutron detector was placed during the capture γ-ray measurements).

Capture γ-ray measurements with and without a gold standard (5.5 cm diam×0.17 cm length) were also made, the former to determine the absolute number of neutrons incident on the ^{13}C sample and the latter to determine the background. These two and the ^{13}C measurements were

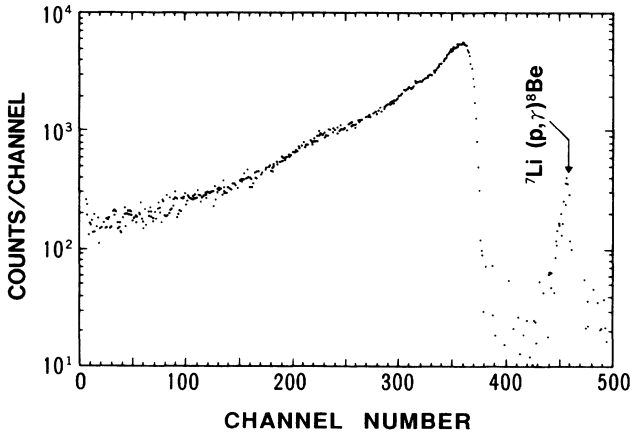

FIG. 3. Neutron time-of-flight spectrum measured by the ^6Li-glass scintillation detector moved to 14° with respect to the direction of the proton beam. The flight path for this run was 37.1 cm and the flight time 0.666 ns/channel.

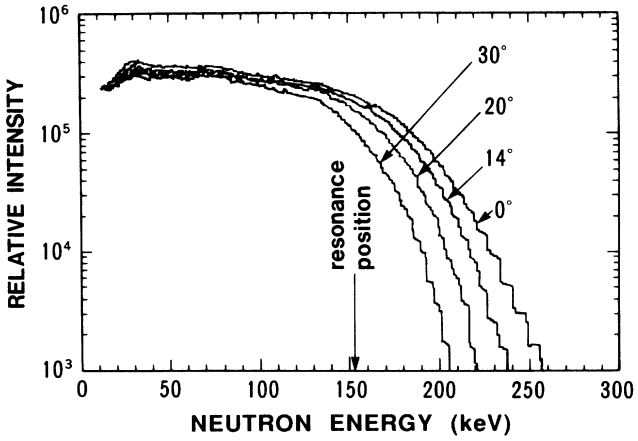

FIG. 4. Relative neutron spectra at various angles deduced from the measured spectra (similar to Fig. 3) and calculated neutron detector efficiencies.

made cyclically to average out changes in experimental conditions and were connected by the monitor counts of the ^{6}Li-glass detector at 30°.

The TOF spectrum of γ-ray events from the ^{13}C sample is shown in Fig. 5(a) and an enlargement (on a linear scale) is shown in Fig. 5(b). The spectrum from gold is shown in Fig. 5(c). The peak P in Fig. 5 is due to the ^{7}Li$(p,\gamma)^{8}$Be and ^{7}Li$(p,p'\gamma)^{7}$Li reactions. The peak sought in the current study, that due to γ rays from the 153-keV resonance in ^{13}C, is the very weak bump marked P' in Figs. 5(a) and (b). The strong and wide bump P'' in Fig. 5(c) arises from the ^{197}Au(n,γ) reaction. Four digital windows, indicated by $W1-W4$, were set on the TOF spectrum and the corresponding γ-ray pulse-height (PH) spectra were stored in a minicomputer. The window $W1$ was set to measure off-resonance capture. The net area above the dashed line [drawn to guide the eye under P' in Fig. 5(b)] in the window $W2$ results from genuine ^{13}C resonance capture. The tail of the large peak P influences both $W1$ and $W2$; therefore, $W3$ was set to determine this background tail. Finally, $W4$ gave information on the (nearly) time-independent background, consisting mainly of γ rays from thermal-neutron capture by H, Fe, and Cd contained in the detector shield and from natural background.

C. Data processing

The measured γ-ray PH spectra from the ^{13}C measurement are shown in Figs. 6(a)–(d) and labeled in the upper right hand corner by the corresponding digital windows. (Note that the window widths differ from window to window.) Peaks due to γ rays from the 153-keV resonance capture can be seen especially in the high-energy region of Fig. 6(b). The background-subtracted PH spectra, W_1(net) and W_2(net), were constructed as follows:

$$W_1(\text{net}) = W_1 - f_1^4 W_4 - t_1^3 (W_3 - f_3^4 W_4) , \quad (1)$$

and

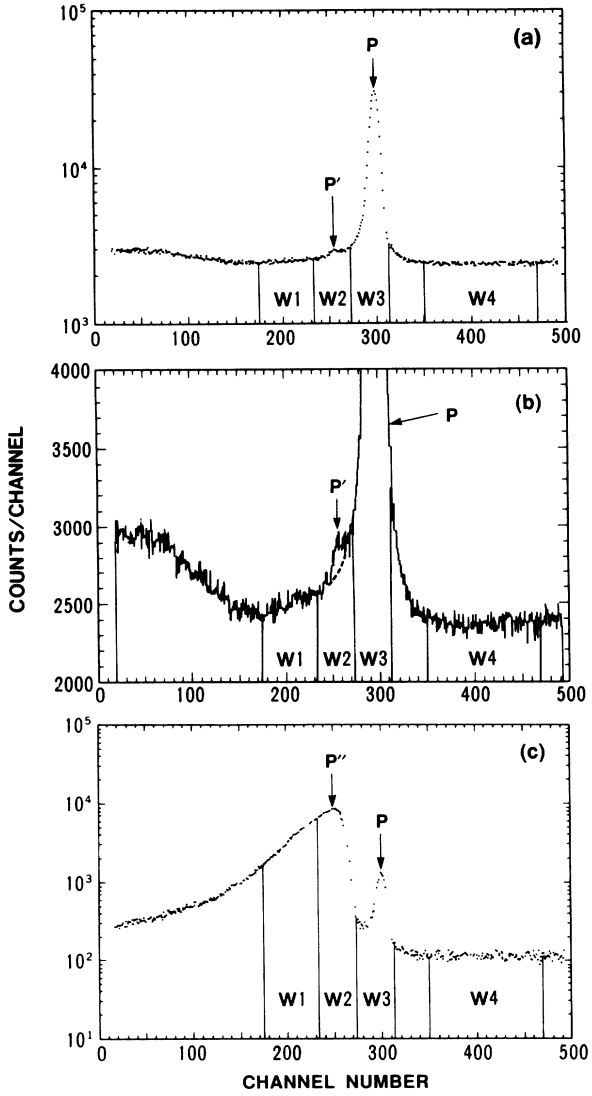

FIG. 5. Time-of-flight (0.354 ns/channel) spectra measured by the γ-ray detector: (a) spectrum from ^{13}C, (b) enlarged figure of (a) on a linear vertical scale, and (c) spectrum from gold. Four digital windows ($W1-W4$) were set on all spectra. The origins of the peaks P, P', and P'' are described in the text.

$$W_2(\text{net}) = W_2 - f_2^4 W_4 - t_2^3 (W_3 - f_3^4 W_4) . \quad (2)$$

Here f_i^j is the width ratio of the ith window to the jth window, and $t_1^3(t_2^3)$ is the ratio of the tail area in $W1(W2)$ to the peak area in $W3$. The t_1^3 and t_2^3 values were determined from the shape of the TOF spectrum (similar to Fig. 5) taken with no sample. The resulting net PH spectra are shown in Figs. 7(a) and 7(b). The three expected primary transitions at 8.32, 2.22, and 1.59 MeV (see Fig. 1) and the two secondary transitions at 6.09 and 6.73 MeV are seen clearly in Fig. 7(b) and weakly, if at all, in Fig. 7(a). We neither expected nor found evidence for significant population of levels at 6.59, 6.90, 7.01, and 7.34 MeV (see Fig. 1); transitions connected to these levels are not discussed any further in this section.

Though the intensities of the 2.22-MeV and 6.09-MeV

transitions are expected to be nearly equal (see Fig. 1), the 2.22-MeV photopeak will appear larger due to the higher detector efficiency at the lower energy. Even then, $\approx 50\%$ of the 2.22-MeV peak in Fig. 7(b) and a greater fraction of $\approx 90\%$ in Fig. 7(a) are not due to genuine 2.22-MeV transitions in ^{14}C; instead they are due to the 2.22-MeV background γ rays from the ^{1}H (thermal n,γ) reactions in the detector shield. Such an incomplete background subtraction [carried out with the aid of the $W4$ spectrum of Fig. 6(d)] is to be expected because the background radiation is only approximately time independent. The peaks at 0.87 and 3.68 MeV in Fig. 7(b) result from the $^{16}O(n,\gamma)$ and $^{12}C(n,\gamma)$ reactions, respectively. These assignments were made with the aid of a separate capture γ-ray measurement with an empty sample holder.

The net counts N_{1f} and N_{2f} of each peak due to the $^{13}C(n,\gamma)$ reaction were extracted from the W_1(net) and W_2(net) spectra, respectively, and are listed in Table I. The net count N_{1f} consists of not only the (dominant) contributions from the off-resonance capture but also the (small) contributions from capture in the tail of the 153-keV resonance. Similarly, N_{2f} consists of both the resonance and off-resonance contributions. The net counts, N_{1f} and N_{2f} may be expressed as follows:

$$N_{1f}=(N_{1f})_{RC}+(N_{1f})_{ORC}\ , \tag{3}$$

and

$$N_{2f}=(N_{2f})_{RC}+(N_{2f})_{ORC}\ . \tag{4}$$

Here, the subscripts RC and ORC denote contributions from the 153-keV resonance capture and off-resonance capture, respectively.

Partial capture cross sections σ_{1f} (or relative yields of

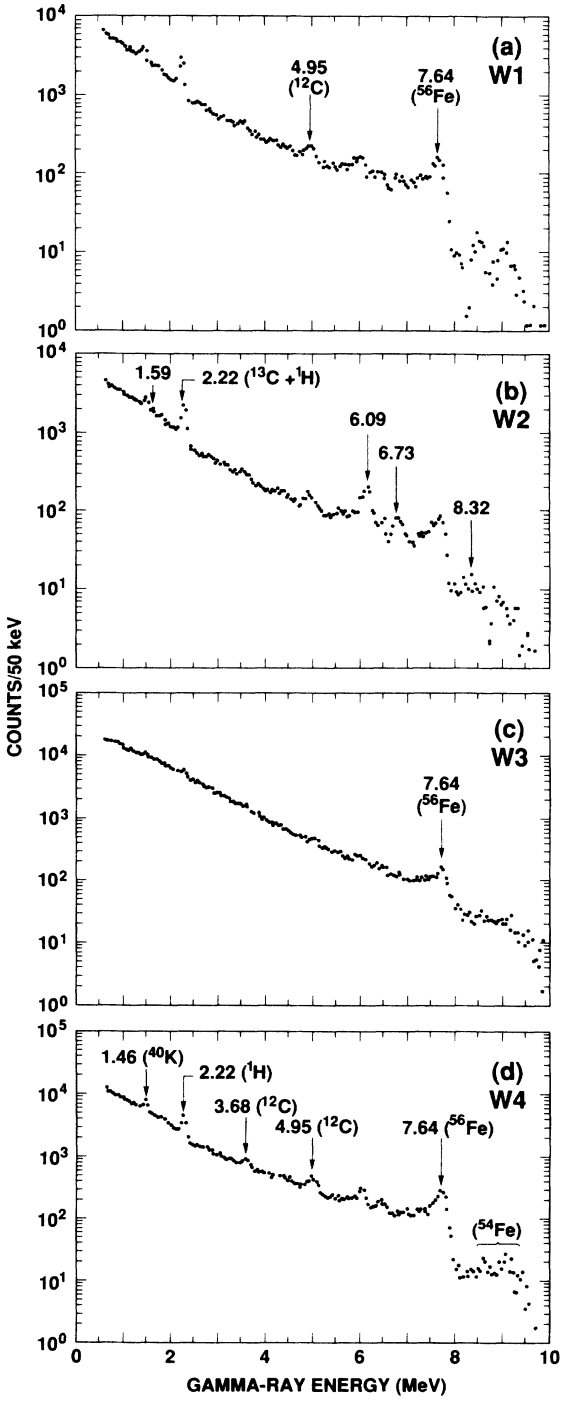

FIG. 6. Gamma-ray pulse-height spectra, labeled by the corresponding digital windows (W), from ^{13}C capture. Peaks due to ^{13}C (See Table I) are indicated in (b); interfering peaks due to the ^{40}K natural background and due to thermal neutron capture in the surrounding material are marked in (d).

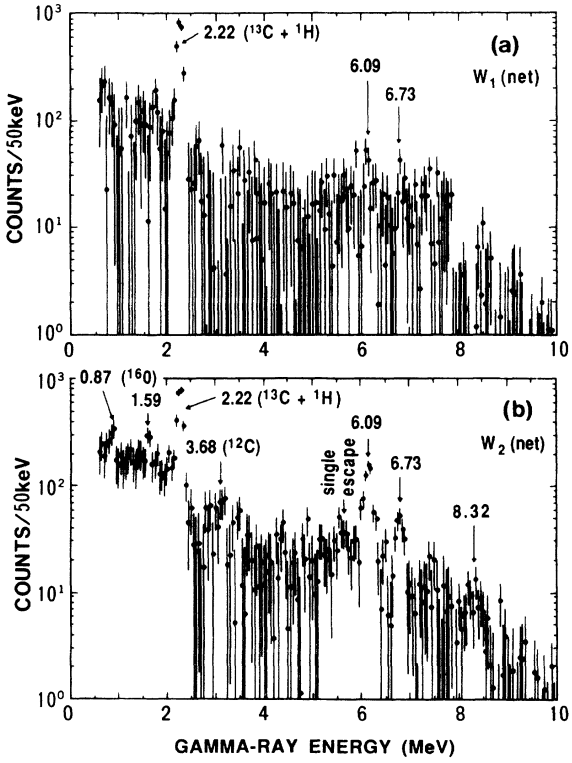

FIG. 7. Background-subtracted γ-ray spectra from ^{13}C: (a) spectrum for the digital window $W1$ (off-resonance capture), and (b) spectrum for $W2$ (153-keV resonance capture).

TABLE I. Gamma rays observed from the 153-keV resonance and off-resonance capture by ^{13}C.

E_γ[a] (MeV)	Transition[a]	N_{1f}[b] (counts)	N_{2f}[b] (counts)	σ_{1f}[c] (μb)	$(\Gamma_f)_{INT}$[d] (meV)	$(\sigma_{1f})_{RC}$[e] (μb)	$(\sigma_{1f})_{ORC}$[f] (μb)	$(\sigma_{2f})_{ORC}$[g] (μb)	Γ_f[h] (meV)	Final Γ_f[i] (meV)
8.32	8.32→0.0	17±18	61±10	3.7±4.0	43±8	0.25±0.05	3.5±4.0	1.5±1.6	34±13	34^{+13}_{-6}
6.73	6.73→0.0	64±29	190±25	11.0±5.1	107±15	0.64±0.09	10.4±5.1	21±10	30±30	
6.09	6.09→0.0	87±38	590±37	13.6±5.9	303±24	1.81±0.14	11.8±5.9	24±10	152±76	
2.22	8.32→6.09	(2310±114)[j]	(2280±94)[j]				(11.5±5.9)[k]		(151±76)[k]	151^{+76}_{-33}
1.59	8.32→6.73	−30±87	421±72	≤4.4	105±19	0.61±0.11	≤4	≤8	(30±30)[l]	30^{+30}_{-13}
								Total off-resonance capture cross section (in μb)		20±9
								Total radiation width (in meV)		215^{+84}_{-35}

[a]See Fig. 1.
[b]Extracted from the spectra shown in Fig. 7.
[c]See Eq. (5).
[d]See Eqs. (6) and (7).
[e]Calculated using $(\Gamma_f)_{INT}$ and the Breit-Wigner single-level formula.
[f]Obtained by subtracting $(\sigma_{1f})_{RC}$ from σ_{1f}.
[g]Calculated using the computer code HIKARI (Ref. 26).
[h]See Eq. (8).
[i]Taking also into account the area of the peak in the TOF spectrum.
[j]Including major contributions due to thermal-neutron capture in ^1H that are incompletely subtracted.
[k]Deduced from the yield of the 6.09-MeV transition after subtracting the small feeding from the 6.73-MeV level (see Fig. 1).
[l]Deduced from the yield of the 6.73-MeV transition.

γ rays) were deduced from the formula

$$\sigma_{1f}=N_{1f}/(C_1 n\varepsilon_f\phi_1) , \quad (5)$$

where C_1 is a correction factor discussed below (the subscript of C denoting the corresponding window) and n the thickness of the ^{13}C sample. The γ-ray detector efficiencies ε_f were determined experimentally[31] employing γ rays from several calibrated sources and from the $^{9}Be(p,\gamma)^{10}B$, $^{19}F(p,\alpha\gamma)^{16}O$, and $^{27}Al(p,\gamma)^{28}Si$ reactions. The number of neutrons in the digital window $W1$ incident on the sample, ϕ_1, was extracted using a pulse-height weighting technique[35] from (1) the capture γ-ray PH spectrum in the gold measurement, (2) the relative incident neutron spectrum measured by the ^{6}Li-glass detector, and (3) the ENDF/B-V (Ref. 34) neutron capture cross section of ^{197}Au. Interim values for the partial radiation widths (or relative yields of γ rays) from the 153-keV resonance, $(\Gamma_f)_{\rm INT}$, were also deduced from the formula

$$N_{2f}=C_2 n\varepsilon_f\phi_2\alpha g\frac{\Gamma_n(\Gamma_f)_{\rm INT}}{\Gamma} , \quad (6)$$

with

$$\alpha=\int_0^\infty \pi\lambda\!\!\!^{-}(E)^2\frac{\Gamma\eta_2(E)}{(E-E_R)^2+(\frac{1}{2}\Gamma)^2}dE , \quad (7)$$

where C_2 is a correction factor, ϕ_2 the number of neutrons in $W2$ incident on the sample, g the statistical factor, Γ_n the neutron width of the resonance, Γ the total width of the resonance, E_R the energy of the resonance, $\eta_2(E)$ the normalized neutron flux distribution in the digital window $W2$, and $\lambda\!\!\!^{-}$ the de Broglie wavelength of the incident neutron with energy E. This distribution was extracted from the relative incident neutron spectrum measured by the ^{6}Li-glass detector, and ϕ_2 was extracted in the same way as ϕ_1. The required resonance parameters were obtained from Ref. 20. The partial-capture cross sections σ_{1f} and the interim values for the partial radiation widths $(\Gamma_f)_{\rm INT}$ are listed in Table I. The 153-keV resonance contributions to the partial-capture cross sections, $(\sigma_{1f})_{\rm RC}$, were calculated using these interim values for the partial radiation widths and the Breit-Wigner single-level formula. The off-resonance partial-capture cross sections, $(\sigma_{1f})_{\rm ORC}$, were obtained by subtracting $(\sigma_{1f})_{\rm RC}$ from σ_{1f}. Both $(\sigma_{1f})_{\rm RC}$ and $(\sigma_{1f})_{\rm ORC}$ are listed in Table I. It can be seen there that the 153-keV resonance contributions are small compared to the off-resonance contributions.

To determine the off-resonance capture cross sections in the window $W2$, the partial direct-capture cross sections of ^{13}C were calculated at the average neutron energies $\bar{E}_{W1}=40$ keV and $\bar{E}_{W2}=150$ keV in the two windows $W1$ and $W2$. These calculations were made with the computer code HIKARI (Ref. 36) based on the distorted-wave Born approximation (DWBA). Relative yields for cascade γ rays were also calculated from these partial cross sections and the known decay scheme (see Fig. 1). The DWBA calculations employed the Moldauer[37] optical potential and the (d,p) spectroscopic factors (see Fig. 1) deduced by Datta *et al.*[26] for the ground state of ^{14}C and by Peterson *et al.*[27] for all other levels. The calculated cross sections are quite sensitive to these physical quantities, but the ratios of the values at $\bar{E}_{W1}$ to the corresponding values at $\bar{E}_{W2}$ are not. Therefore, we normalized the calculated cross sections to the observed off-resonance partial-capture cross sections $(\sigma_{1f})_{\rm ORC}$, and further assumed that the off-resonance partial-capture cross sections $(\sigma_{2f})_{\rm ORC}$ at $\bar{E}_{W2}$ were represented by the normalized values at $\bar{E}_{W2}$. The resulting $(\sigma_{2f})_{\rm ORC}$ values are also listed in Table I.

The off-resonance contribution $(N_{2f})_{\rm ORC}$ was calculated using the above $(\sigma_{2f})_{\rm ORC}$ values, and the resonance-capture contribution $(N_{2f})_{\rm RC}$ was extracted using Eq. (4). Finally, the partial radiation widths of the 153-keV resonance, Γ_f, were deduced from the formula

$$(N_{2f})_{\rm RC}=C_2 n\varepsilon_f\phi_2\alpha g\frac{\Gamma_n\Gamma_f}{\Gamma} , \quad (8)$$

where α has been defined by Eq. (7) and the other quantities have been already explained below Eqs. (6) and (7). These Γ_f values are listed in the tenth column of Table I.

The total radiation width of the 153-keV resonance and the total off-resonance capture cross section in window $W1$ ($\bar{E}_{W1}=40$ keV) are also listed in Table I. In arriving at these values, we assumed that the total radiation width (the total cross section) was the sum of the partial radiation widths (the partial cross sections) for the three primary transitions at 8.32, 2.22, and 1.59 MeV shown in Fig. 1.

Corrections[33] were made for the neutron self-shielding in the sample (C_{ns}), multiple scattering in the sample (C_{nm}), γ-ray absorption in the sample (C_{ga}), and the dependence of the γ-ray detection efficiency on the γ-ray source position (C_{sp}). The total correction factor of Eqs. (5), (6), and (8) is defined as

$$C=C_{ns}C_{nm}C_{ga}C_{sp} . \quad (9)$$

The total correction factor and its components are listed in Table II for various windows. A small correction ($\sim$3%) for the angular distribution of the 8.32-MeV, $E2$ transition was also made assuming no interference between resonance and off-resonance capture.

The uncertainties quoted for the final results given in the eighth and tenth columns of Table I take into account not only the counting statistics but also the uncertainties due to several factors: (1) 3–7% in the γ-ray detector efficiency, (2) $\sim$10% in the relative neutron spectrum incident on the sample, (3) $\sim$5% in the capture cross section of ^{197}Au, and (4) 5–10% in extracting the net peak-area count N_{1f} or N_{2f} from the PH spectrum. Despite a total running time of 70 h, the uncertainty in the net count N_{1f}, resulting predominantly from the counting statistics, is very large (see Table I) and propagates into both the off-resonance and the 153-keV resonance results. A straightforward error analysis leads to symmetric uncertainties for the measured radiation widths listed in the tenth column of Table I; imposing the constraint that the 153-keV resonance was definitely observed in the TOF spectrum [see Fig. 5(b)] leads to the asymmetrical uncer-

TABLE II. Correction factors used [see Eq. (9)] in the data analyses.

Sample	Window	C_{ns}	C_{nm}	C_{ga}	C_{sp}	C
^{13}C	$W1$	0.92	1.16	0.97–0.98	0.99	1.03–1.04
^{13}C	$W2$	0.75	1.15	0.97–0.98	0.99	0.82–0.83
^{197}Au	$W1$	0.94	1.20	~0.90	0.99	~1.01
^{197}Au	$W2$	0.95	1.16	~0.90	0.99	~0.98

tainties given in the last column of Table I.

It is possible to check further on the validity of the partial and total radiation widths measured in this experiment as follows. In Fig. 5(b), the net counts above the dashed line in the window $W2$ results from genuine 153-keV resonance capture and represent (mainly) the cumulative contribution from the five transitions listed in Table I. The result was 2030±330 counts. The separate contribution from each transition is $R_f(N_{2f})_{\rm RC}$, where $(N_{2f})_{\rm RC}$ is the same quantity appearing in Eqs. (4) and (8), and R_f is the ratio of the total γ-ray detection efficiency to the full-energy peak efficiency ε_f. The quantity R_f does depend on the γ-ray energy and was determined from the response function of the γ-ray detector,[31] taking into consideration the PH discrimination level used in obtaining the TOF spectrum shown in Fig. 5(b). The resulting sum of the contributions from the five transitions was 2470±930 counts (compared to the net 2030±330 counts), thus validating the current results.

The total radiation width of $0.215^{+0.084}_{-0.035}$ eV deduced from the current experiment with a NaI(Tl)-based detection system is much smaller than the previous value of 2.4±0.9 eV obtained with a C_6F_6-based detection system. Our result suggests that in the previous measurement either the scattered-neutron sensitivity of the system was underestimated or the pulse-height weighting of the data was done incorrectly or both.

III. CALCULATION OF THE VALENCE RADIATION WIDTH

A. Theory

Our aim in this section is to model the wave function for resonance elastic scattering in terms of the single-particle state of a real potential that is similar to the real part of a global optical potential and to determine the valence radiation width from this modeling. The description of the scattering is made within the $\mathcal{R}$-matrix theory. The fractionation of the modeled single-particle state into the actual resonance is known from the neutron width of the resonance determined experimentally. It is therefore unnecessary, in this approach, to model the expected average fractionation by the formulation of the imaginary part of the optical model. We thus avoid any uncertainties arising from such a modeling.

Beyond the range of the nuclear forces, the wave function for a unit flux, plane wave of neutrons impinging on and interacting with a target nucleus can be written as

$$\psi_{\rm ext}=\frac{i\sqrt{\pi}}{kr\sqrt{v}}\sum_J\sum_{j=|I-J|}^{I+J}\sum_{l=|j-(1/2)|}^{j+(1/2)}\sum_M\left[\mathcal{I}_{0JM;lj}-\sum_{vj'l'}U^{(J)}_{vj'l';0jl}\mathcal{O}_{vJM;l'j'}\right]\cdot \tag{10}$$

Here, k is the wave number of the relative motion of projectile and target, v is their relative velocity, and r is their radial separation. Components of the total angular momentum are denoted by J (magnetic quantum number M), the coupled spin-orbit angular momentum (the coupled sum of orbital angular momentum l and neutron spin σ) by j, and the target nucleus spin by I. These quantum numbers, together with the state of excitation v of the target (normally in its ground state denoted by 0) define the entrance channel. The incoming motion within this channel is described by the wave function $\mathcal{I}_{0JM;lj}$. As a result of the nuclear interactions, there are outgoing waves $\mathcal{O}_{vJM;l'j'}$ in channels with the residual nucleus in a state of excitation denoted by v, and a set of angular-momentum quantum numbers that are differentiated from those of the entrance channel by primes. Generally, the collective set of quantum numbers for the general case is abbreviated into the single index c for the entrance channel, and c' for the outgoing channels. The amplitudes of the outgoing waves in the various exit channels are given by the elements $U_{c'c}$ of the collision matrix.

The external region beyond the range of nuclear forces in which the wave function $\psi_{\rm ext}$ [see Eq. (10)] is appropriate can be defined by setting suitable channel radii a_c in all channels. When the radial separation between target and projectile (or residual and ejectile) is less than the channel radius (in all channels), the compound system is defined as being within the internal region. The wave function within this region is denoted by $\psi_{\rm int}$ and is smoothly connected to $\psi_{\rm ext}$ in all channels. The overall wave function of the reacting system is therefore

$$\begin{aligned}&\psi=\psi_{\rm int}\quad\text{for } r_c<a_c\ (\text{all } c)\ ;\\&\psi=\psi_{\rm ext}\quad\text{for } r_c\geq a_c\ (\text{in channel } c)\ .\end{aligned}\tag{11}$$

The cross section for radiative capture is obtained from this wave function by forming the matrix element of the

electromagnetic perturbation term $\mathcal{H}'$ in the Hamiltonian between this initial state and a final state Φ_μ. The transition probability, and hence the cross section, is given by

$$T=\sigma_{n\gamma(\to\mu)}=\frac{2\pi\rho}{\hbar}|\langle\Psi|\mathcal{H}'|\Phi_\mu\rangle|^2 , \tag{12}$$

where ρ is the density of photon states. After expanding the perturbation operator as a sum of electric and magnetic multipole terms, the cross section for electric-dipole transitions is found to be

$$\sigma_{n\gamma(\to\mu)}=\frac{16\pi}{9}\frac{k_\gamma^3 e^2}{\hbar}\left[\frac{Z}{A}\right]^2|\langle\Psi|rY_{1\mathcal{M}}|\Phi_\mu\rangle|^2 \tag{13}$$

for photons of polarization quantum number $\mathcal{M}$. In Eq. (13), k_γ is the photon wave number, e the electric charge, and $Y_{1\mathcal{M}}$ a spherical harmonic of the order 1. The symbols Z and A denote, as usual, the proton and mass numbers of the nucleus. For obtaining the total capture cross section in an unpolarized system, this expression is summed over all magnetic substates of the final state irrespective of photon polarization, and averaged over all magnetic substates of the initial state. With separation of the radial and angle-spin factors of the matrix element, the cross section becomes

$$\sigma_{n\gamma(\to\mu)}=\frac{16\pi}{9}\frac{k_\gamma^3 e^2}{\hbar}\left[\frac{Z}{A}\right]^2|\langle\Psi|r|\Phi_\mu\rangle|^2\frac{|\langle J\|\mathbf{Y}_1\|J_\mu\rangle|^2}{(2J+1)} \tag{14}$$

for each component of total angular momentum J of the initial system. Evaluation of the reduced matrix element, assuming that the system is coupled according to the neutron spin-orbit angular scheme outlined in the preceding paragraph, gives

$$\frac{|\langle J\|\mathbf{Y}_1\|J_\mu\rangle|^2}{(2J+1)}=\frac{1}{4\pi}(2J_\mu+1)(2j+1)(2j'+1)(2l+1)(2l'+1)W^2(jJj'J_\mu;I1)W^2(ljl'j';\tfrac{1}{2}1)(l0l'0|ll'10)^2 , \tag{15}$$

where W is the recoupling coefficient of Racah and $(j_1m_1j_2m_2|j_1j_2j_3m_3)$ is the vector coupling coefficient. We write the right-hand side of Eq. (15) as

$$(3/4\pi)\mathcal{W}_{J_\mu J'l',Jjl} .$$

The wave function ψ_{int} may now be described in terms of $\mathcal{R}$-matrix basls states that are, as usual, defined as discrete eigenstates X_λ (with eigenvalues E_λ) satisfying the Schrödinger equation for the full Hamiltonian in the internal region and constrained by constant real boundary conditions at the channel radii a_c. Partial neutron widths $\Gamma_{\lambda(c)}$ are associated with each eigenstate. These are expressed as the product of a penetration factor $2P_c$ and reduced width $\gamma^2_{\lambda(c)}$. The reduced width amplitude $\gamma_{\lambda(c)}$ is proportional to the amplitude, at the channel radius, of the eigenfunction X_λ projected onto the channel wave function. Under the conditions that all reaction channel widths $\Gamma_{\lambda(c')}$ are small compared to the separation between levels, the diagonal collision matrix element for elastic scattering has the form

$$U_{cc}=e^{-2i\phi_c}(1+iP_c\mathcal{R}_{cc})/(1-iP_c\mathcal{R}_{cc}) , \tag{16}$$

where ϕ_c is the hard-sphere phase shift and $\mathcal{R}_{cc}$ the reduced diagonal $\mathcal{R}$-matrix element for channel c. Equation (16) is valid provided the boundary conditions at the channel radii are set equal to the values of the real parts of the logarithmic derivatives of the outgoing waves (the shift factors). The reduced $\mathcal{R}$ matrix is expressed in terms of the eigenstates X_λ by

$$\mathcal{R}_{cc}=\sum_\lambda\frac{\gamma^2_{\lambda(c)}}{E_\lambda-E-\frac{1}{2}i\sum_{c'\neq c}\Gamma_{\lambda(c')}} . \tag{17}$$

Equations (16) and (17) are written implicitly for a specific value of total angular momentum J and parity π, and the set of levels λ employed in Eq. (17) is specific for these two quantum numbers. The incomplete sum of the partial widths in the denominator of Eq. (17) is henceforth denoted by $\Gamma_{\lambda(e)}$.

The internal wave function corresponding to the collision function [see Eqs. (10) and (16)] is proportional to

$$\frac{\pi^{1/2}\hbar^{1/2}e^{-i\phi_c}}{k}\frac{2^{1/2}P_c^{1/2}}{1-iP_c\mathcal{R}_{cc}}\sum_\lambda\frac{\gamma_{\lambda(c)}X_\lambda}{E_\lambda-E-\frac{1}{2}i\Gamma_{\lambda(e)}} , \tag{18}$$

the constant of proportionality being the combination of vector coupling coefficients for linking spins to total angular momentum J through the spin-orbit coupling scheme.

After substitution of these various expressions in terms of $\mathcal{R}$-matrix eigenfunctions into the wave function Ψ, we obtain for Eq. (14)

$$\sigma_{n\gamma(\to\mu)}=\frac{\pi}{k^2}\frac{16\pi k_\gamma^3 e^2}{9}\left[\frac{Z}{A}\right]^2\sum_{J^\pi}g_J\frac{3}{4\pi}\mathcal{W}_{J_\mu J'l',Jjl}\left|\Omega\sum_\lambda\frac{\Gamma^{1/2}_{\lambda(0IJ)}\langle X_\lambda|r|\Phi_\mu\rangle}{E_\lambda-E-\frac{1}{2}i\Gamma_{\lambda(e)}}+\Omega P_l\mathcal{R}_{cc}\left\langle\frac{\mathcal{I}_l e^{i\phi_l}+\mathcal{O}_l e^{-i\phi_l}}{\hbar^{1/2}v^{1/2}}\,\middle|\,r\,\middle|\,\Phi_\mu\right\rangle\right.$$
$$\left.+i\Omega\left\langle\frac{\mathcal{I}_l e^{i\phi_l}-\mathcal{O}_l e^{-i\phi_l}}{\hbar^{1/2}v^{1/2}}\,\middle|\,r\,\middle|\,\Phi_\mu\right\rangle\right|^2 , \tag{19}$$

where Ω is the quantity $e^{-i\phi_l}/(1-iP_l\mathcal{R}_{cc})$ and $\mathcal{I}_l(r)$, $\mathcal{O}_l(r)$ are the radial factors in the channel wave functions $\mathcal{I}_{0JM;lj}$, $\mathcal{O}_{\nu JM;l'j'}$; they are expressed in terms of spherical Bessel and Neumann functions as

$$\mathcal{I}_l(r)=-kr[n_l(kr)+ij_l(kr)] , \tag{20}$$

and

$$\mathcal{O}_l(r)=-kr[n_l(kr)-ij_l(kr)] . \tag{21}$$

In evaluating the first matrix element of Eq. (19), the integral is confined to the internal region; all others to the channel $r>a_c$. Strictly, there should be other terms within the modulus brackets of Eq. (19) corresponding to matrix elements in other (reaction) channels, but these are omitted here because we are aiming at calculating the cross sections within the entrance-channel valence model. The internal radial matrix element is now to be understood as being confined to the projection of the wave function X_λ and Φ_μ on the channel configurations $0j$ and $0j'$, respectively; that is, the single-particle components of these states. We denote these projected wave functions by $X_\lambda(r)$ and $\Phi_\mu(r)$, respectively.

If the last term (that corresponding to capture from hard-sphere scattering) in the modulus brackets of Eq. (19) is now neglected, the remaining expression corresponds to resonance valence capture. If a single level is dominant, we can compare this expression with the Breit-Wigner single-level formula

$$\sigma_{n\gamma(\mu)}=\frac{\pi}{k^2}g_J\frac{\Gamma_{\lambda(0lj)}\Gamma_{\lambda(\gamma\to\mu)}}{(E_\lambda-E)^2+(\frac{1}{2}\Gamma_\lambda)^2} \tag{22}$$

to obtain the radiation width expression

$$\Gamma_{\lambda(\gamma\to\mu)}=\frac{4k_\gamma^3\mathcal{W}_{J_\mu j'l',Jjl}}{3}\left[\frac{Z}{A}\right]^2\frac{e^2}{\hbar v}2P_l\gamma^2_{\lambda(0lj)}\left|\left[\frac{P_0}{P_l}\right]^{1/2}\left\langle\frac{X_\lambda(r)}{X_\lambda(a)}\middle|r\middle|\Phi_\mu(r)\right\rangle_{\text{int}}+\left\langle\frac{\mathcal{I}_le^{i\phi_l}+\mathcal{O}_le^{-i\phi_l}}{2}\middle|r\middle|\Phi_\mu(r)\right\rangle_{\text{ext}}\right|^2 . \tag{23}$$

Note that continuity of the radial integrands of the matrix elements across the channel boundary is ensured by the relation

$$\mathcal{I}_l(a)e^{i\phi_l}+\mathcal{O}_l(a)e^{-i\phi_l}=2(P_0/P_1)^{1/2} , \tag{24}$$

and that the radiation width does not have a threshold neutron energy dependence.

The valence radiation width of Eq. (23) is proportional to the reduced neutron width whose value, in turn, depends on the channel radius through the normalization of the eigenstate X_λ. We avoid the problem of normalization involved in the choice of channel radius by calculating the ratio $\Gamma_{\lambda(\gamma\to\mu)}/2P_l\gamma^2_{\lambda(0lj)}$ in the following way. We determine a single-particle $\mathcal{R}$-matrix model state, appropriate to the actual resonance energy E_λ, orbital angular momentum l, and coupled spin j (surmised if not known) for the case under study by solving the radial Schrödinger equation for a real potential with radius R, diffuseness parameter d, and spin-orbit coupling strength similar to those of a realistic optical-model potential for the corresponding target nucleus and energy region. The solution is constrained by imposing the boundary condition $B=S_l$ where S_l is the real part of the logarithmic derivative of O_l; i.e.,

$$S_l+iP_l=L_l=\frac{a}{\mathcal{O}_l(a)}\left[\frac{\partial\mathcal{O}_l}{\partial r}\right]_{r=a} \tag{25}$$

at a channel radius a chosen beyond the cutoff point of the Woods-Saxon potential. We normally take a linear cutoff region for the potential. This region starts from a point, usually chosen as $r'=R+6d$. Here the Woods-Saxon potential form ceases, falls linearly in magnitude to zero, and ends at a point $r''=r'+d$; hence $a\geq r''$. The number of nodes of the single-particle state is specified, and the potential depth is varied until an eigensolution is found at the specified resonance energy; the radial wave function of this state is denoted by $u_i(r)$. The same procedure is adopted for the final state radial wave function ω_f with its specified values of binding energy, orbital angular momentum l', and coupled spin j', but with the boundary and normalization conditions appropriate to a naturally attenuating wave function in the channel. From the two wave functions generated for these states, the quantity

$$\frac{\Gamma_{i(\gamma\to f)}}{2P_l\gamma^2_{i(0lj)}}=\frac{4k_\gamma^3\mathcal{W}_{J_f j'l',Jjl}}{3}\left[\frac{Z}{A}\right]^2\frac{e^2}{\hbar v}\left|\left[\frac{P_0}{P_l}\right]^{1/2}\left\langle\frac{u_i(r)}{u_i(a)}\middle|r\middle|\omega_f(r)\right\rangle+\left\langle\frac{\mathcal{I}_le^{i\phi_l}+\mathcal{O}_le^{-i\phi_l}}{2}\middle|r\middle|\omega_f(r)\right\rangle\right|^2 \tag{26}$$

is calculated. The reduced width of this state is

$$\gamma^2_{i(0lj)}=\left[\frac{\hbar^2}{2ma}\right]u_i(a)^2 , \tag{27}$$

where m is the reduced mass of the neutron-target system. Now for the actual $\mathcal{R}$-matrix state that describes the resonance within the single-level approximation, we assume

$$X_\lambda(r)=c_{\lambda,i(0lj)}u_i(r) , \tag{28}$$

and for the actual final state

$$\Phi_\mu(r)=\theta_{\mu,f(0l'j')}\omega_f(r)\ , \tag{29}$$

where c and θ are expansion coefficients for core single-particle configurations of the compound nucleus. Therefore,

$$\gamma^2_{\lambda(0lj)}=\left[\frac{\hbar^2}{2ma}\right]c^2_{\lambda,i(0lj)}u_l(a)^2\ , \tag{30}$$

and

$$\frac{\Gamma_{\lambda(\gamma\to\mu)}}{2P_l\gamma^2_{\lambda(0lj)}}=\frac{\theta^2_{\mu,f(0l'j')}\Gamma_{i(\gamma\to f)}}{2P_l\gamma^2_{i(0lj)}}\ . \tag{31}$$

Thus the valence radiation width for the resonance is obtained by multiplying the calculated quantity of Eq. (26) by the experimentally known quantities; namely, the (d,p) spectroscopic factor of the final state and the neutron width $\Gamma_{\lambda(n)}=2P_l\gamma^2_{\lambda(0lj)}$ of the resonance.

B. Specific calculations for ^{13}C

The resonance at 153-keV neutron energy has spin and parity $J^\pi=2^+$, and orbital angular momentum $l=1$. Its neutron width is 3.7±0.7 keV. There are three states at lower excitation that are reached by electric-dipole transitions from this resonance (see Fig. 1 and Sec. II). The lowest at 6.09 MeV is mainly $s_{1/2}$ single-particle in character, and those at 6.73 and 7.34 MeV are essentially $d_{5/2}$ single-particle states.

The matrix element calculations were based on the optical-model parameters of Moldauer[37] (with no imaginary term included). This potential employs a Woods-Saxon form

$$\mathcal{V}(r)=\mathcal{V}_0/\{1+\exp[(r-R)/d]\}+(\boldsymbol{l}\cdot\boldsymbol{\sigma})K_s\mathcal{V}_0\exp[(r-R)/d](rd)^{-1}\{1+\exp[(r-R)/d]\}^{-2}\ . \tag{32}$$

The numerical value for the potential radius is $R=(1.16A^{1/3}+0.6)$ fm, giving $R=3.328$ fm for ^{13}C, while the diffuseness parameter is $d=0.62$ fm. For the spin-orbit coupling strength, we use the value $K_s=0.435$ (fm)^2. The well depth $\mathcal{V}_0$ was adjusted in our calculation to reproduce the resonance energy of the initial state or the binding energy of the final state in each of the three transitions studied.

1. *Capture to the 6.09 MeV state*

If the single-particle component of the 153-keV resonance is assumed to be of $1p_{3/2}$ character, the potential depth $\mathcal{V}_0$ required to given an $\mathcal{R}$-matrix state at this neutron energy is approximately -18 MeV, the precise value depending on the value taken for the channel radius. If it is assumed to be of $2p_{3/2}$ character, $\mathcal{V}_0\approx-63$ MeV. We have carried out calculations for both possibilities.

The 6.09-MeV, $J^\pi=1^-$ state is bound by 2.082 MeV. The potential depth required to give a $2s_{1/2}$ eigenstate at this energy is $\mathcal{V}_0=-46.6$ MeV. The calculated value is

$$\frac{\Gamma_\lambda(\gamma\to\mu)}{2P_l\gamma^2_{\lambda(0lj)}}=0.17\times10^{-3}\theta_f^2\mathcal{W}_{1(1/2)0,2(3/2)1}(1p_{3/2})$$
$$=0.15\times10^{-3}\theta_f^2\mathcal{W}_{1(1/2)0,2(3/2)1}(2p_{3/2})\ .$$

Hence from the values of the spectroscopic factor (see Fig. 1) and the neutron width

$$\Gamma_{\gamma\to6.09}=0.16\text{ eV }(1p_{3/2})$$
$$=0.14\text{ eV }(2p_{3/2})\ .$$

These values are to be compared with the measured value of $0.151^{+0.076}_{-0.033}$ eV for this transition.

2. *Capture to the 6.73 MeV state*

This state is bound by 1.45 MeV and is of $1d_{5/2}$ character. The potential depth required to reproduce this binding energy is $\mathcal{V}_0=-40.7$ MeV. The calculated values for the radiation width are

$$\Gamma_{\gamma\to6.73}=0.47\times10^{-4}\Gamma_n\theta_f^2\mathcal{W}_{3(5/2)2,2(3/2)1}(1p_{3/2})$$
$$=0.064\text{ eV}\ ,$$

or

$$\Gamma_{\gamma\to6.73}=0.24\times10^{-4}\Gamma_n\theta_f^2\mathcal{W}_{3(5/2)2,2(3/2)1}(2p_{3/2})$$
$$=0.033\text{ eV}\ .$$

The measured value is $0.030^{+0.030}_{-0.013}$ eV.

3. *Capture to the 7.34 MeV state*

The binding energy is 0.84 MeV and the single-particle orbit is again $1d_{5/2}$. The calculated values of the radiation width are

$$\Gamma_{\gamma\to7.34}=0.13\times10^{-4}\Gamma_n\theta_f^2\mathcal{W}_{2(5/2)2,2(3/2)1}\ (1p_{3/2})$$
$$=1.4\text{ meV}\ ,$$

or

$$\Gamma_{\gamma\to7.34}=0.74\times10^{-5}\Gamma_n\theta_f^2\mathcal{W}_{2(5/2)2,2(3/2)1}\ (2p_{3/2})$$
$$=0.79\text{ meV}\ .$$

This transition has a vanishingly small width and was not observed in this experiment.

4. *Capture to the ground state*

A number of rather strong $E2$ transitions have been observed to follow thermal-neutron capture by a few nuclides.[29] There has been speculation in the literature[38–40] that these may be of direct character although the mechanism invoked (giving a large effective charge to the neutron) depends on polarization of the core. If $E2$ direct capture occurs, there is likely to be corresponding

valence capture at neutron resonances. In this section, we consider the possibility that the 8.32 MeV $E2$ transition to the ground state, measured in this work as having a radiation width of 34^{+13}_{-6} meV (see Table I), can be explained as a valence transition.

Our definition of a valence transition is one in which the valence nucleon makes a change of its single-particle motion within the potential field of an apparently inert core. In this sense we can carry through the calculation of a neutron electric-quadrupole transition in a manner analogous to the $E1$ case. The matrix elements now have the $E2$ operator $\bar{e}r^2Y_{2M}$ and the effective charge for a neutron is, to first order, eZ/A^2. With this low effective charge, the computation of the valence radiation width for the 8.32-MeV transition gives the value of 2.3 μeV which is more than 4 orders of magnitude smaller than the measured value. Thus we can rule out the simple valence model as an explanation for this transition.

A proton transition within an inert core (of ^{13}B) would, because of its effective charge being almost equal to the actual proton charge, give a width of the order of 1 meV, if the reduced proton width is assumed to be equal to the reduced neutron width. This is still rather small and invites the speculation that the mechanism is a collective transition within the compound system.

IV. IMPLICATIONS FOR NUCLEOSYNTHESIS

The $^{13}C(n,\gamma)^{14}C$ reaction rate is determined mainly by the nonresonant s-wave direct-capture contribution to the ground state of ^{14}C and by the resonant p-wave contribution from the 153-keV, 2^+ resonance. The nonresonant (nr) term can be derived from the measured[19] thermal-neutron capture cross section ($\sigma_{th}=1.37\pm0.04$ mb) as

$$N_A\langle\sigma v\rangle_{nr}=N_A\sigma_{th}v_{th}=182\ \text{cm}^3/\text{mol s}\ , \tag{33}$$

where N_A is the Avogadro constant and v is the velocity of neutrons. The resonant contribution is determined by the resonance strength

$$\omega_\gamma=\frac{(2J+1)}{(2\sigma+1)(2I+1)}\frac{\Gamma_n\Gamma_\gamma}{\Gamma}\ , \tag{34}$$

where J, σ, and I denote the spin of the resonance, neutron, and target nucleus, respectively, and Γ_n, Γ_γ, and Γ correspond to the neutron width, gamma width, and total width of the resonance level. The current value, $\omega\gamma=0.269$ eV, results in a Maxwellian-averaged[41,42] resonant (r) contribution given by

$$N_A\langle\sigma v\rangle_r=4.633\times10^4T_9^{-3/2}\times\exp(-1.636/T_9)\ \text{cm}^3/\text{mol s}\ , \tag{35}$$

where T_9 denotes the temperature in 10^9 K. Figure 8 shows the two contributions to this reaction rate as a function of temperature. At $T_9\geq0.3$, typical for He core burning conditions in red-giant stars, the resonant contribution clearly dominates the reaction rate. The significant reduction in this rate resulting from our work can be seen in Fig. 8 by comparing the dashed and solid lines.

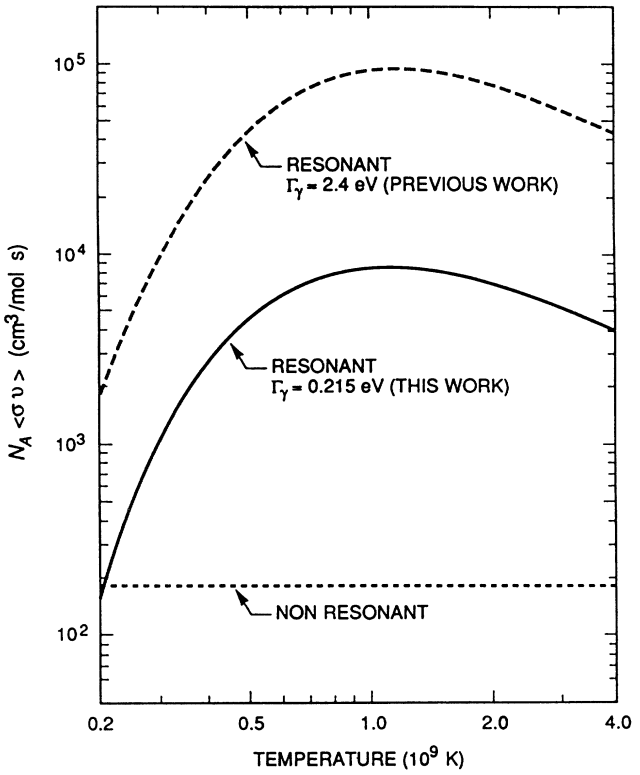

FIG. 8. Reaction rate for $^{13}C(n,\gamma)^{14}C$ based on the current (solid line) and previous (dashed line) values for the total radiation width of the 153-keV resonance. The dotted line is the nonresonant contribution.

How does this reduction, especially at high temperature conditions, affect the s-process nucleosynthesis in red-giant stars,[43] and the r-process nucleosynthesis in a primordial nonstandard Big-Bang environment?[44] The s process takes place during the He-burning phase of stars. The $^{13}C(\alpha,n)^{16}O$ and/or the $^{22}Ne(\alpha,n)^{25}Mg$ reactions are considered to be the two most promising neutron-source candidates for this process at red-giant conditions. However, ^{13}C, which is thought to be mixed into the He-burning zone from the outer CNO-burning layers, might be depleted fairly quickly by the (n,γ) reaction before producing sufficient amounts of neutrons via the competing (α,n) reaction. The equilibrium abundance of ^{13}C in the He-burning core can be written as

$$\langle{}^{13}\text{C}\rangle=\frac{\lambda_{\text{mix}}}{N_\alpha\langle\alpha,n\rangle+N_n\langle n,\gamma\rangle}\ , \tag{36}$$

where N_α and N_n are the alpha and neutron abundances in the burning zone, respectively; $\langle\alpha,n\rangle$ and $\langle n,\gamma\rangle$ are the corresponding reaction rates; and λ_{mix} is the rate at which ^{13}C is mixed into the core.

Typical neutron abundances in red-giant cores vary between 10^9 and 10^{10} n/cm^3 (Ref. 43), while the He abundances are approximately between 10^{23} and 10^{26} α/cm^3 depending on the core density. Even with the fairly small rate for the $^{13}C(\alpha,n)^{16}O$ reaction,[45] this reaction dominates neutron capture by several orders of magnitude be-

cause of the low neutron abundances under these conditions. Therefore, the current measurement has little significance for the He-burning scenario.

The possibility of a primordial r process in terms of a nonstandard Big-Bang model has been discussed recently.[44,46] The mass 5 and mass 8 instability gaps are bridged by the reaction sequence

$$^{7}\mathrm{Be}(n,p)^{7}\mathrm{Li}(n,\gamma)^{8}\mathrm{Li}(\alpha,n)^{11}\mathrm{B}\ .$$

This path allows sufficient mass flow (not possible at standard Big-Bang conditions) towards heavier $A \geq 12$ elements. However, the reaction rate for the trigger reaction $^{7}\mathrm{Li}(n,\gamma)$ has been measured recently[47] and found to be significantly smaller than previously suggested. The main production line for the heavier isotopes has been identified[48] as

$$^{11}\mathrm{B}(n,\gamma)^{12}\mathrm{B}(\beta^{-}\nu)^{12}\mathrm{C}(n,\gamma)^{13}\mathrm{C}(n,\gamma)^{14}\mathrm{C}\cdots\ ,$$

with the alternative branch as

$$^{12}\mathrm{B}(n,\gamma)^{13}\mathrm{B}(\beta^{-}\nu)^{13}\mathrm{C}(n,\gamma)^{14}\mathrm{C}\cdots\ .$$

Both reaction sequences will lead to the production of ^{13}C during nonstandard Big-Bang nucleosynthesis. The depletion of ^{13}C and, therefore, the production of higher mass elements depends on the neutron capture rate of ^{13}C at Big-Bang temperatures $T_9 = 0.8$ to 1.0 and densities of 10^{-4} to 10^{-5} g/cm^3. The considerable reduction of this rate, as determined in the current experiment, will significantly reduce the production of $A \geq 14$ isotopes during primordial nucleosynthesis.

V. SUMMARY

Measurements of radiation widths of the resonances in cross sections of light nuclides are difficult to make and are rather sparse. The p-wave resonance in the neutron cross section of ^{13}C is of particular interest, but it seemed likely, on theoretical grounds, that the existing value of its radiation width was wrong by a large factor. A remeasurement of the total radiation width was therefore undertaken through the determination of its components for the principal primary γ transitions. The total radiation width, $0.215^{+0.084}_{-0.035}$ eV, is more than one order of magnitude smaller than the previously accepted value. This total is dominated by an $E1$ transition with a partial width of $0.151^{+0.076}_{-0.033}$ eV to the 6.09-MeV state in ^{14}C. A second $E1$ transition to the 6.73 MeV state has a width of $0.030^{+0.030}_{-0.013}$ eV, while a third expected transition to the 7.34-MeV state is found to be so weak as to be unobservable in these measurements. There is also a surprisingly strong $E2$ transition to the ^{14}C ground state with a partial width of $0.034^{+0.0013}_{-0.006}$ eV.

It is found that the $E1$ transitions can all be explained as simple neutron valence transitions, the model calculations agreeing with the measured values within experimental uncertainties. The $E2$ transition is much too strong, however, to be a strict neutron valence transition. It is probably too strong even to be attributed to a single-proton transition, unless the proton channel from this resonance has an exceptionally large reduced width.

Of the two possible scenarios for nucleosynthesis—red-giant He burning and nonstandard Big Bang—the current measurement has negligible impact on the former, but affects the latter in terms of a significant reduction in the production of $A \geq 14$ isotopes.

ACKNOWLEDGMENTS

S.R. is grateful to the Japan Atomic Energy Research Institute (JAERI) at Tokai-mura for its generous hospitality during the summer of 1986 and during subsequent visits under the U.S. Department of Energy (DOE)/JAERI Coöperative Program in Nuclear Physics. J.E.L. wishes to express similar sentiments to the Argonne National Laboratory and the University of Chicago. The authors thank Y. K. Ho and B. Castel for helpful correspondence, J. W. Jury for loaning us the target material, and M. Wiescher for elucidating the implications of our measurements for nucleosynthesis. They also thank R. R. Winters and R. L. Macklin for helpful comments on the manuscript. The current research was sponsored in part by the DOE under Contract No. DE-AC05-84OR21400 with Martin Marietta Energy Systems, Inc. (Oak Ridge) and Contract No. W-31-109-Eng-38 with the University of Chicago (Argonne).

*Permanent address: U.K.A.E.A., Harwell, England.

[1]S. Raman, R. F. Carlton, J. C. Wells, E. T. Jurney, and J. E. Lynn, Phys. Rev. C **32**, 18 (1985).

[2]S. Raman and J. E. Lynn, in *Proceedings of the Fourth International Symposium on Neutron-Induced Reactions, Smolenice, Czechoslovakia, 1985,* edited by J. Krištiak and E. Běták (Veda, Bratislava, 1986), p. 253.

[3]J. E. Lynn, S. Kahane, and S. Raman, Phys. Rev. C **35**, 26 (1987).

[4]S. Kahane, J. E. Lynn, and S. Raman, Phys. Rev. C **36**, 533 (1987).

[5]S. Raman, S. Kahane, and J. E. Lynn, in *Proceedings of the Sixth International Symposium on Capture Gamma-Ray Spectroscopy, Leuven, Belgium, 1987,* Institute of Physics Conf. Series No. 88, edited by P. Van Assche and K. Abrahams (Institute of Physics, Bristol 1988) [J. Phys. G **14**, Suppl. S223 (1988)].

[6]S. Raman, S. Kahane, and J. E. Lynn, in *Proceedings of the International Conference on Nuclear Data for Science and Technology, Mito, Japan, 1988,* edited by S. Igarasi (Saikon, Tokyo, 1988), p. 645.

[7]S. Raman, S. Kahane, R. M. Moon, J. A. Fernandez-Baca, J. E. Lynn, and J. W. Richardson, Jr., Phys. Rev. C **39**, 1297 (1989).

[8]S. F. Mughabghab, R. E. Chrien, O. A. Wasson, G. W. Cole, and M. R. Bhat, Phys. Rev. Lett. **26**, 1118 (1971).

[9]S. Raman, G. G. Slaughter, J. C. Wells, Jr., and B. J. Allen, Phys. Rev. C **22**, 328 (1980).

[10]J. P. Mason, Harwell Report AERE R 12078, 1986 (unpublished); and in Proceedings of the International Conference

on Nuclear Physics, Harrogate, 1986 (unpublished), Vol. 1, p. 341.
[11]H. Weigmann, S. Raman, J. A. Harvey, R. L. Macklin, and G. G. Slaughter, Phys. Rev. C **20**, 115 (1979).
[12]B. Gyarmati, A. M. Lane, and J. Zimanyi, Phys. Lett. **50B**, 316 (1974).
[13]T. Uchiyama and H. Morinaga, Z. Phys. A **320**, 273 (1985).
[14]A. M. Lane and J. E. Lynn, Nucl. Phys. **17**, 563 (1960); **17**, 586 (1960).
[15]A. M. Lane and S. F. Mughabghab, Phys. Rev. C **10**, 412 (1974).
[16]R. F. Barrett and T. Terasawa, Nucl. Phys. **A240**, 445 (1975).
[17]J. E. Lynn, *The Theory of Neutron Resonance Reactions* (Clarendon, Oxford, 1968), p. 326.
[18]A. M. Lane and R. G. Thomas, Rev. Mod. Phys. **30**, 257 (1958).
[19]S. F. Mughabghab, M. Divadeenam, and N. E. Holden, *Neutron Cross Sections* (Academic, New York, 1981), Vol. 1, p. 6-3. The listed energy of 173.6 keV for the second resonance in ^{13}C is incorrent. The correct value is 1736 keV.
[20]H. T. Heaton II, J. L. Menke, R. A. Schrack, and R. B. Schwartz, Nucl. Sci. Eng. **56**, 27 (1975).
[21]B. J. Allen and R. L. Macklin, Phys. Rev. C **3**, 1737 (1971).
[22]B. J. Allen, A. R. de L. Musgrave, R. L. Macklin, and R. R. Winters, in *Proceedings of a Specialist's Meeting on Neutron Data of Structural Materials for Fast Reactors, Geel, Belgium, 1977,* edited by K. H. Böckhoff (Pergamon, New York, 1978), p. 506.
[23]R. L. Macklin, private communication.
[24]Y. K. Ho and B. Castel, private communication; Y. K. Ho, Chin. Phys. Lett. **4**, 7 (1987).
[25]F. Ajzenberg-Selove, Nucl. Phys. **A449**, 1 (1986).
[26]S. K. Datta, G. P. A. Berg, and P. A. Quin, Nucl. Phys. **A312**, 1 (1978).
[27]R. J. Peterson, H. C. Bhang, J. J. Hamill, and T. G. Masterson, Nucl. Phys. **A425**, 469 (1984).
[28]C. M. McCullagh, M. L. Stelts, and R. E. Chrien, Phys. Rev. C **23**, 1394 (1981).
[29]S. Raman, in *Proceedings of the Fourth International Symposium on Neutron-Capture Gamma-Ray Spectroscopy and Related Topics, Grenoble, 1981,* Institute of Physics Conf. Series No. 62, edited by T. von Egidy, F. Gönnenwein, and B. Maier (Institute of Physics, Bristol, 1982), p. 357.
[30]P. M. Endt, At. Data Nucl. data Tables **23**, 3 (1979); **23**, 547 (1979); **26**, 47 (1981).
[31]M. Igashira, H. Kitazawa, M. Shimizu, H. Komano, and N. Yamamuro, Nucl. Phys. **A457**, 301 (1986).
[32]M. Igashira, H. Kitazawa, and N. Yamamuro, Nucl. Instrum. Methods Phys. Res. **A245**, 432 (1986).
[33]Based partly on the Monte Carlo code described by J. G. Sullivan, G. G. Warner, R. C. Block, and R. W. Hockenbury, Rensselaer Polytechnic Institute Report RPI-328-155, 1969.
[34]ENDF/B-V data file for ^{6}Li (MAT=1303) evaluated by G. Hale, L. Stewart, and P. G. Young (unpublished) and for ^{197}Au (MAT=1379) evaluated by S. F. Mughabghab (unpublished).
[35]R. L. Macklin and J. H. Gibbons, Phys. Rev. **159**, 1007 (1967).
[36]H. Kitazawa, Triangle Universities Nuclear Laboratory Annual Report TUNL-XIX, 1980, p. 114.
[37]P. A. Moldauer, Nucl. Phys. **47**, 65 (1963).
[38]W. V. Prestwich and T. J. Kennett, Phys. Rev. C **30**, 392 (1984).
[39]B. Castel and Y. K. Ho, Phys. Rev. C **34**, 408 (1986).
[40]Y. K. Ho and C. Coceva, in *Proceedings of the Sixth International Symposium on Capture Gamma-Ray Spectroscopy, Leuven, Belgium, 1987,* Institute of Physics Conf. Series No. 88, edited by P. Van Assche and K. Abrahams (Institute of Physics, Bristol, 1988) [J. Phys. G **14**, Suppl. S207 (1988)].
[41]Z. Y. Bao and F. Käppeler, At. Data Nucl. Data Tables **36**, 411 (1987).
[42]R. R. Winters and R. L. Macklin, Astrophys. J. **313**, 808 (1987).
[43]N. Prantzos, M. Arnould, and J. P. Arcoragi, Astrophys. J. **315**, 209 (1987).
[44]G. J. Mathews, G. M. Fuller, and C. R. Kajino, in Proceedings of the 8th Moriond Astrophysics Meeting, Les Arcs, France, 1988 (unpublished).
[45]G. R. Caughlan, W. A. Fowler, M. J. Harris, and B. A. Zimmerman, At. Data Nucl. Data Tables **32**, 197 (1985).
[46]G. M. Fuller, G. J. Mathews, and C. R. Alcock, in *The Origin and Distribution of Elements,* edited by G. J. Mathews (World Scientific, Singapore, 1987), p. 36.
[47]M. Wiescher, R. Steininger, and F. Käppeler, Astrophys. J. **344**, 464 (1989).
[48]R. A. Malaney and W. A. Fowler, Astrophys. J. **333**, 14 (1988).